Physics Letters B 754 (2016) 104–108

Contents lists available at ScienceDirect

Physics Letters B

www.elsevier.com/locate/physletb

Spallation reaction study for fission products in nuclear waste: Cross section measurements for ^{137}Cs and ^{90}Sr on proton and deuteron

H. Wang [a,*], H. Otsu [a], H. Sakurai [a], D.S. Ahn [a], M. Aikawa [b], P. Doornenbal [a], N. Fukuda [a], T. Isobe [a], S. Kawakami [c], S. Koyama [d], T. Kubo [a], S. Kubono [a], G. Lorusso [a], Y. Maeda [c], A. Makinaga [e], S. Momiyama [d], K. Nakano [f], M. Niikura [d], Y. Shiga [g,a], P.-A. Söderström [a], H. Suzuki [a], H. Takeda [a], S. Takeuchi [a], R. Taniuchi [d,a], Ya. Watanabe [a], Yu. Watanabe [f], H. Yamasaki [d], K. Yoshida [a]

[a] RIKEN Nishina Center, 2-1 Hirosawa, Wako, Saitama 351-0198, Japan
[b] Faculty of Science, Hokkaido University, Sapporo 060-0810, Japan
[c] Department of Applied Physics, University of Miyazaki, Miyazaki 889-2192, Japan
[d] Department of Physics, University of Tokyo, 7-3-1 Hongo, Bunkyo, Tokyo 113-0033, Japan
[e] Graduate School of Medicine, Hokkaido University, North-14, West-5, Kita-ku, Sapporo 060-8648, Japan
[f] Department of Advanced Energy Engineering Science, Kyushu University, Kasuga, Fukuoka 816-8580, Japan
[g] Department of Physics, Rikkyo University, 3-34-1 Nishi-Ikebukuro, Toshima, Tokyo 171-8501, Japan

ARTICLE INFO

Article history:
Received 27 August 2015
Received in revised form 14 December 2015
Accepted 29 December 2015
Available online 11 January 2016
Editor: D.F. Geesaman

Keywords:
Spallation reaction on proton and deuteron
Transmutation of long-lived fission products
^{137}Cs
^{90}Sr

ABSTRACT

We have studied spallation reactions for the fission products ^{137}Cs and ^{90}Sr for the purpose of nuclear waste transmutation. The spallation cross sections on the proton and deuteron were obtained in inverse kinematics for the first time using secondary beams of ^{137}Cs and ^{90}Sr at 185 MeV/nucleon at the RIKEN Radioactive Isotope Beam Factory. The target dependence has been investigated systematically, and the cross-section differences between the proton and deuteron are found to be larger for lighter spallation products. The experimental data are compared with the PHITS calculation, which includes cascade and evaporation processes. Our results suggest that both proton- and deuteron-induced spallation reactions are promising mechanisms for the transmutation of radioactive fission products.

1. Introduction

Nuclear power has provided a modern source of energy since the middle of the twentieth century. Because the nuclear power stations do not produce greenhouse gases, nuclear power is considered as a potential candidate to mitigate climate change while delivering a large amount of energy. However, nuclear safety and security are matters of concern to the entire world. Reduction in the quantity of high-level radioactive waste is one of the major issues for the use of a nuclear power plant.

Research and development into the reduction of radioactive waste using partitioning and transmutation technology has been performed over recent decades [1]. High-level radioactive waste has two main components: long-lived fission product (LLFP) and minor actinide (MA). The transmutation of MA has been studied in detail for the purpose of reprocessing spent nuclear fuel in a concept of using the accelerator-driven system (ADS) [2]. For instance, proton/deuteron-induced spallation reactions of heavy stable nuclei have been investigated at GSI for ADS targets [3,4]. On the other hand, the transmutation of LLFP has not been studied as extensively because they are not considered to be useful materials for power production. In addition, LLFP can be produced continuously in ADS systems and next-generation nuclear reactors, for instance fast breeder reactors.

However, the transmutation on ^{137}Cs and ^{90}Sr, which have large weight fractions (40%) in LLFP, has received much attention. These two isotopes have large radiotoxicities due to their relatively short half lives of 30 years [5]. Indeed, their radiotoxicities are predominant (more than 90%) in the first 100 years after the reprocessing of spent fuel. In addition, these two LLFP nuclei are the major source of heat in high-level nuclear waste [1]. ^{137}Cs and ^{90}Sr have

* Corresponding author.
E-mail address: wanghe@ribf.riken.jp (H. Wang).

http://dx.doi.org/10.1016/j.physletb.2015.12.078

small thermal neutron-capture cross sections [6,7] and, therefore, it is essential to find other effective reactions for their transmutation. The possibility of proton-induced spallation reaction has been discussed in Refs. [8,9]; however, experimental reaction data are currently lacking.

Nuclear physics plays an essential role in addressing the treatment on LLFP, because the reliable reaction data and models are necessary for LLFP reactions. Thanks to the radioactive isotope beams, the mechanisms of spallation reactions of LLFP nuclei on proton and deuteron can be investigated. Because the proton–proton and proton–neutron interaction cross sections are known to be different, it is therefore important to study the cross-section differences in long-lived fission products to clarify the reaction mechanisms. To this end, the reaction energy around 200 MeV/nucleon was chosen in the present study to observe differences in the cross sections measured with the proton and deuteron targets, because the proton–proton interaction cross section (σ_{pp}) is significantly smaller than the proton–neutron (σ_{pn}) one at this reaction energy. The high quality data of production cross sections for the interaction of LLFP with possible transmutation targets are critical to converge towards a solution for transmutation of long-lived waste, as well as to verify the fragmentation and/or spallation models.

In this Letter, we report results from the first attempt to study the spallation reaction of the fission products ^{137}Cs and ^{90}Sr in the aspect of nuclear waste transmutation for LLFP. The inverse reaction technique was adopted in the present work: fast radioactive beams of ^{137}Cs and ^{90}Sr, produced at the in-flight separator BigRIPS [10,11] of the RIKEN Radioactive Isotope Beam Factory (RIBF) [12], were used and proton/deuteron-induced reactions were conducted using proton and deuteron targets. The technique allows us to study systematically the target dependence of reactions at an energy of ∼185 MeV/nucleon — the typical energy of beams delivered by the in-flight separator — and to identify unambiguously spallation products for isotopic production cross section measurements. In addition, the technique avoids the difficulties associated with using a highly radioactive target.

2. Experiment

The experiment was performed at RIBF, operated by RIKEN Nishina Center and the Center for Nuclear Study, University of Tokyo. The secondary beams were produced from in-flight fission of a ^{238}U primary beam at 345 MeV/nucleon on a 1-mm-thick Be target located at the object point of the BigRIPS fragment separator. The average primary beam intensity was about 12 particle nA. In the present studies, the total intensities of the secondary beams were restricted to fit the requirement of the data acquisition system. The BigRIPS settings were optimized to obtain the ^{137}Cs and ^{90}Sr beams with high purities. The momentum acceptance of BigRIPS was set to be 0.1% by using the slits at the dispersive focal plane. Two secondary beam settings were applied, which were optimized for the transmission of ^{137}Cs and ^{90}Sr, respectively. Secondary cocktail beams were selected and purified by employing two wedge-shaped aluminum energy degraders at the dispersive foci. Degraders with thicknesses of 1.35 and 0.26 g/cm^2 were used for the ^{137}Cs setting, while the 1.88- and 1.35-g/cm^2-thick degraders were adopted for the ^{90}Sr setting. The beam energies were both 185 MeV/nucleon in front of the secondary targets. Particles in the secondary beams were identified event-by-event via the TOF-$B\rho$-ΔE method, which is described in Refs. [13,14], using similar detectors and devices. The main contaminants in the ^{137}Cs and ^{90}Sr settings were the $N = 82$ isotone ^{136}Xe and $N = 52$ isotone ^{91}Y, respectively. Thanks to the excellent resolving power in in-flight particle identification of BigRIPS [14], the interested isotopes ^{137}Cs and ^{90}Sr were well separated from others in the secondary beams and were clearly selected for the data analysis. The typical intensities of the ^{137}Cs and ^{90}Sr beams were 1.2×10^3 and 7.1×10^3 particles per second, with purities of 14% and 28%, respectively.

Three targets, 179.2-mg/cm^2 CH_2, 217.8-mg/cm^2 CD_2 [15], and 226.0-mg/cm^2 ^{12}C, were used to induce the secondary reactions; the thicknesses were chosen so that the energy losses of both secondary beams were similar in each target. Therefore, data could be obtained for all targets using a common setting for the ZeroDegree spectrometer [11]. Uncertainties of the thicknesses, determined by weight measurement, were less than 2%. In order to obtain the background contribution, data were accumulated using the target holder with no target inserted.

The reaction residues were measured by the ZeroDegree spectrometer with a full momentum acceptance (6%) and full angular acceptances in both the horizontal (90 mrad) and vertical (60 mrad) directions. In order to cover a broad range of spallation products, several different magnetic rigidity ($B\rho$) settings were applied: −9%, −6%, −3%, 0%, and +3% relative to the $B\rho$ value of the secondary beam. Thus, a sufficient overlap was obtained for neighboring settings. The momentum distributions of the products were obtained by the $B\rho$ measurement at the dispersive focus of the ZeroDegree spectrometer. After the secondary reactions, the width of the momentum distribution was less than 1%, which was smaller than the momentum acceptance. The angular spreads of the products were estimated to be less than 6 mrad (9 mrad) for the ^{137}Cs (^{90}Sr) case based on the Goldhaber model [16] including the deflection effect [17]. This model might give an overestimation for the width of momentum distributions of products in both the proton- and deuteron-induced spallation reactions, as shown in Refs. [4,18]. Thus, such angular spreads were much smaller than the angular acceptance of the ZeroDegree spectrometer. For safety, the momentum acceptance was limited to be $\Delta p/p \leq \pm 2.5\%$ in the analysis to ensure the full acceptances in both angle and momentum [19] in each $B\rho$ setting.

The particle identification in the ZeroDegree spectrometer was achieved by measuring the time of flight (TOF), $B\rho$, energy loss (ΔE), and total kinetic energy (TKE). The TOF information was obtained between two plastic scintillators, one placed at the entrance and the other at final focus of ZeroDegree. A trajectory reconstruction was applied to determine the $B\rho$ value using position and angle measurements at the dispersive focus. The ΔE value was measured by an ionization chamber located at the final focal plane. The detection efficiencies of the tracking procedure and the ion chamber were higher than 95%. The TKE measurement was made by a cylinder-shaped $LaBr_3$(Ce) scintillator [20] placed downstream of the ionization chamber. The atomic number Z, mass-to-charge ratio A/Q, and mass number A, were obtained from ΔE-TOF, $B\rho$-TOF, and TKE-TOF correlations, respectively.

The particle identification plot for reaction products in the ZeroDegree spectrometer from the ^{137}Cs secondary beam is shown in Fig. 1. Fig. 1(a) displays a two-dimensional plot of Z versus A/Q for the products produced from ^{137}Cs on the carbon target. The resolutions in Z and A/Q for both the Cs and Sr isotopes were 0.47 (FWHM) and 4.8×10^{-3} (FWHM), respectively. The plot contains contributions from products that are not fully stripped, namely, hydrogen-like ($Q = Z - 1$) and helium-like ($Q = Z - 2$) charge states. Fig. 1(b) shows a two-dimensional plot of A versus A/Q for the Cs isotopes that lie within $Z = 55 \pm 0.5$, as indicated by the horizontal dashed lines in Fig. 1(a). The resolution in A for the Cs isotopes was 1.9 (FWHM), which is sufficient to unambiguously distinguish the fully stripped ions from the other charge states, as shown in Fig. 1(b).

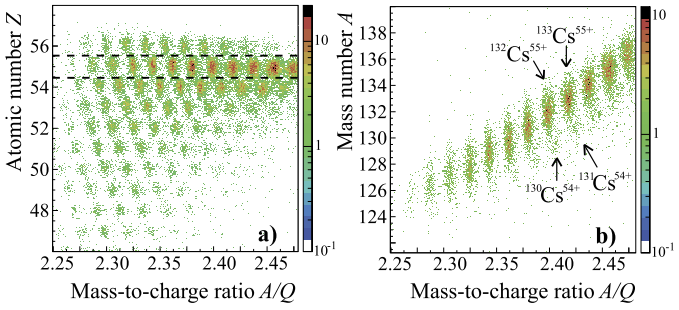

Fig. 1. (Color online.) Particle identification plots for reaction residues produced from the ^{137}Cs beam deduced using the ZeroDegree spectrometer. Panel (a) displays a two-dimensional plot of Z versus A/Q. The horizontal dashed lines indicate the gate limits on Z to select the Cs isotopes. In Panel (b), the two-dimensional plot of A versus A/Q is shown for the Cs isotopes. The fully stripped ions are clearly separated from the $Q = Z - 1$ events.

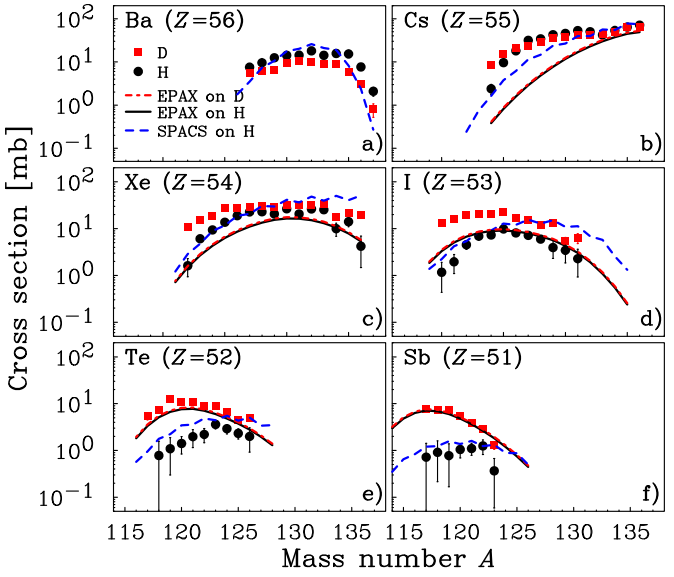

Fig. 2. (Color online.) Isotopic distributions of the measured cross sections for $51 \leq Z \leq 56$ elements produced by ^{137}Cs on proton (circle) and deuteron (square) at 185 MeV/nucleon. The solid and dot-dashed lines indicate EPAX [22] calculations on proton and deuteron, respectively, and these two EPAX calculations are close to each other. The SPACS [23] calculations on proton (dashed) is also displayed for comparison.

After passing through the carbon target, the fractions of ions in the $Q = Z$, $Q = Z - 1$, and $Q = Z - 2$ charge states were 78%, 21%, and 1%, respectively, for the Cs isotopes. The reaction residues from ^{90}Sr were clearly separated and identified in the ZeroDegree spectrometer without using the TKE information and the charge-state contribution was less than 1%.

3. Results and discussion

The spallation cross sections measured in the present work for the ^{137}Cs and ^{90}Sr beams using proton and deuteron targets are plotted in Figs. 2 and 4, respectively. The respective cross sections were deduced from the CH_2 and CD_2 targets after subtracting contributions from carbon (using data from the C target run) and beam-line materials (using data from the empty-target run). Each panel in Figs. 2 and 4 displays the cross sections for one element ($51 \leq Z \leq 56$ and $34 \leq Z \leq 39$ for the ^{137}Cs and ^{90}Sr beams, respectively) as a function of mass number. The cross section measurement was limited up to 1 mb because of statistics.

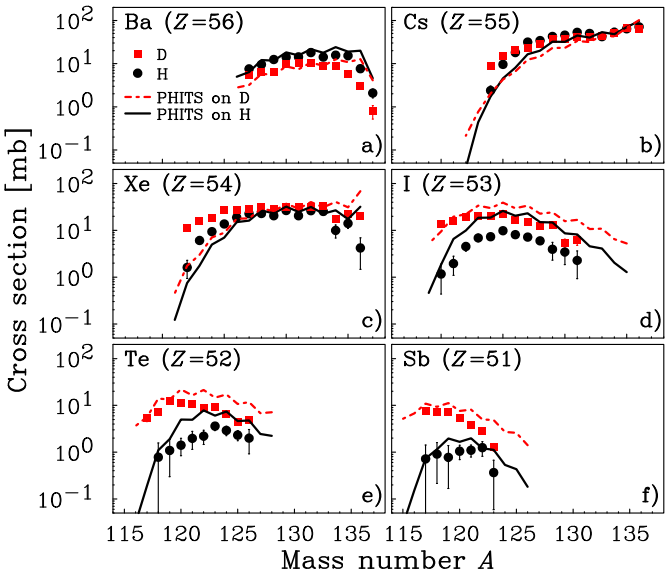

Fig. 3. (Color online.) Isotopic distributions of the measured cross sections for $51 \leq Z \leq 56$ elements produced by ^{137}Cs on proton (circle) and deuteron (square) at 185 MeV/nucleon. The PHITS [24] calculations on proton (solid) and deuteron (dot-dashed) are displayed for comparison.

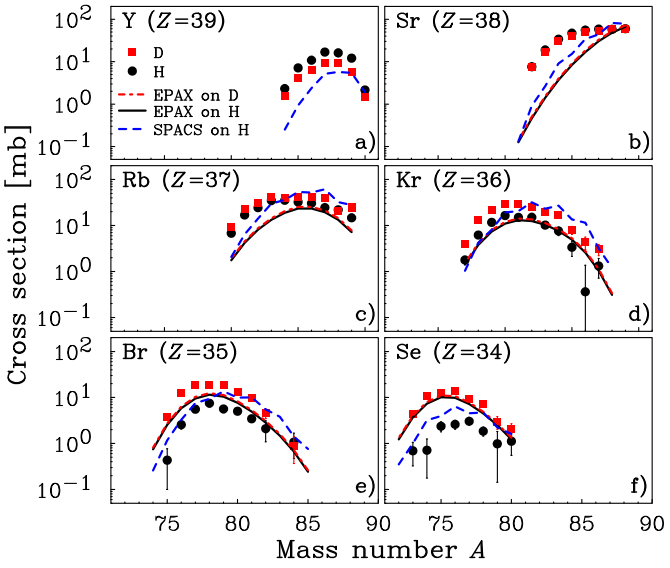

Fig. 4. (Color online.) Same as Fig. 2, but for $34 \leq Z \leq 39$ elements produced by ^{90}Sr.

Figs. 2(a) and 4(a) correspond to the charge-exchange reactions. In this channel, the proton-induced cross sections (σ_p) are larger than the deuteron-induced ones (σ_d). At a high reaction energy, a similar trend was observed in the charge-exchange reaction of ^{136}Xe [21]. For the products close in Z to the projectiles, which are displayed in Panels (b) and (c) in Figs. 2 and 4, both σ_d and σ_p remain almost constant over a wide range of mass numbers, and then slightly decrease for the neutron-deficient nuclei. The isotopic distributions displayed in Panels (d)–(f) in Figs. 2 and 4 show bell-shaped distributions, namely, the cross sections decrease from a maximum towards both the neutron-rich and neutron-deficient sides; σ_d is larger than σ_p and their difference generally becomes more significant for the lighter products.

In order to understand the isotopic distribution cross section quantitatively, three calculations were chosen for comparison, which are also plotted in Figs. 2–5. They are the EPAX [22] empir-

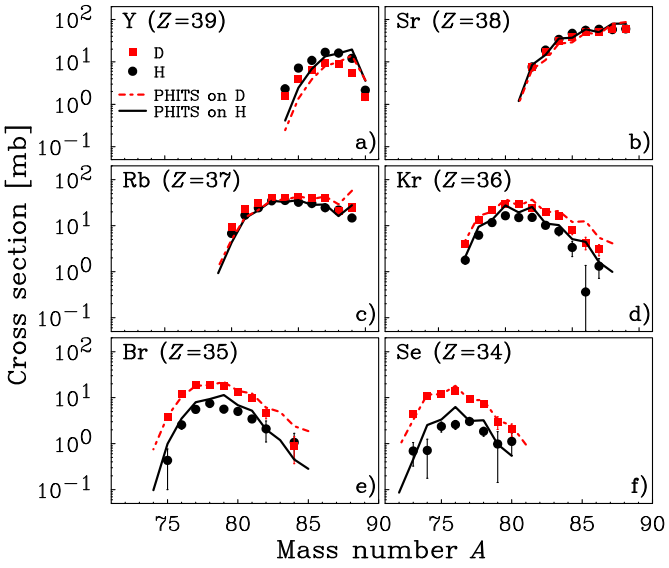

Fig. 5. (Color online.) Same as Fig. 3, but for $34 \leq Z \leq 39$ elements produced by ^{90}Sr.

ical formula, the new semi-empirical parameterization SPACS [23] which is developed to suit proton- and neutron-induced spallation reactions, and an intra-nuclear cascade and evaporation model using the particle and heavy ion transport code system (PHITS) [24]; the cascade and evaporation processes were simulated by using the Intranuclear Cascade model of Liège (INCL) [25] and the generalized evaporation model (GEM) [26], respectively.

The EPAX predictions are systematically smaller than the experimental results for the spallation products in Panels (b) and (c) of Figs. 2 and 4, particularly for the Cs and Sr isotopic chains. These products were produced via the so-called "very peripheral reaction" [27], where neutron evaporation dominates [18]. Underestimated cross sections by EPAX have also been observed in fragmentation reactions of ^{136}Xe on a ^{9}Be target at 1 GeV/nucleon [27], and ^{86}Kr on ^{181}Ta and ^{9}Be at 64 MeV/nucleon [28]. For the lighter products, EPAX overestimates the proton-induced cross sections, as indicated in Panels (e) and (f) of Figs. 2 and 4. The EPAX calculations were shown just for comparison, because EPAX is widely used for the estimation on the production yields of fragmentation reactions at the in-flight facilities. Note that EPAX fits for the target heavier than ^{9}Be [29]. The SPACS predictions are in a reasonable agreement with the isotopic distribution for the proton-induced cross sections. SPACS overestimates the cross sections in the neutron-rich region for products with $Z = 51$–53 produced from ^{137}Cs, as displayed in Panels (d)–(f) of Fig. 2, and the ones with $Z = 34$–36 produced from ^{90}Sr, as shown in Panels (d)–(f) of Fig. 4. The PHITS calculations generally reproduce the experimental systematic trends. Overestimated cross sections on the neutron-rich sides are found for some low-Z products, such as I, Te, and Sb, as shown in Fig. 3(d)–(f). In addition, the odd–even staggering effect is overestimated by PHITS. To reduce the overestimation of the odd–even staggering, two effects may give contributions. One is the competition between the emission of light particles and γ rays in the evaporation stage [30] and the other is the influence of angular momenta in the level density [31]. Indeed, a reduction of the odd–even staggering is shown by including these two effects in Ref. [23]. Further studies on the INCL + GEM calculations including these two effects are encouraged for a better description on the odd–even staggering in PHITS.

In order to investigate the difference between σ_d and σ_p, their ratios σ_d/σ_p are plotted in Fig. 6 as a function of mass number.

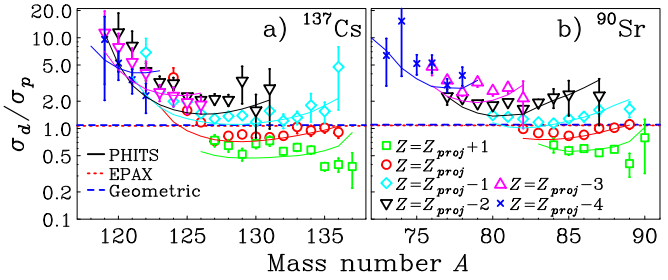

Fig. 6. (Color online.) σ_d/σ_p ratios for products with (a) $51 \leq Z \leq 56$ produced from the ^{137}Cs beam and (b) $34 \leq Z \leq 39$ from the ^{90}Sr beam. The predictions from the EPAX empirical formula (dotted) [22], and theoretical calculations using PHITS (solid) [24] and the geometric model (dashed) [32] are displayed for comparison. Z and Z_{proj} represent the atomic number of the products and projectiles, respectively. See text for details.

A relatively flat ratio is obtained for the isotopic chains close in Z to the projectiles. Furthermore, the ratios increase with the number of protons removed. The ΔZ $(= Z_{proj} - Z)$ dependence might be caused by two effects according to the PHITS calculation. One is that the excitation energy is higher in average in the deuteron-induced reactions than in the proton-induced ones, allowing a large emission of protons and neutrons. The other is related to the large difference between σ_{pn} and σ_{pp}. Neutron in deuteron has more chance to remove protons. More protons are removed from the projectile, when the neutron in deuteron gives contribution to the production. For the light products, a large enhancement (~ 10) is observed towards the neutron-deficient side. It is noted that in the spallation of ^{136}Xe at a higher reaction energy [21], the difference between σ_d and σ_p is less pronounced than what is observed in the present work. This might be because that the difference between σ_{pp} and σ_{pn} reduces when the reaction energy is higher than 185 MeV/nucleon.

The experimental σ_d/σ_p ratios are compared with EPAX, PHITS, and the geometrical model [32] in Fig. 6. Both geometrical and EPAX calculations give constant ratios, around 1.1, for different isotopes. For the charge-exchange reactions, the σ_d/σ_p ratios lie below the geometrical predictions. For the $Z = Z_{proj}$ and $Z = Z_{proj} - 1$ products, the experimental results are similar to the geometrical and EPAX calculations, although EPAX underestimates both σ_d and σ_p, as presented in Panels (b) and (c) of Figs. 2 and 4. The ratios exceed the predictions in the light-mass region by a factor of 10. The proton- and neutron-number dependence of the σ_d/σ_p ratios are reproduced well by PHITS. Following the PHITS prediction, a very large σ_d/σ_p ratio is expected for the lighter products. In the spallation of ^{136}Xe at 500 MeV/nucleon [33], the difference between the deutron- and proton-induced cross sections is also getting larger towards neutron-deficient side within one isotopic chain when $\Delta Z > 2$, although the difference is less pronounced than that in the present work as mentioned above. The difference between σ_d and σ_p is not constant, indicating that the deuteron cannot be understood as a composition of an incoherent proton and neutron [34].

The light products were probably produced via a central collision, where the production cross section depends on the energy deposited. Because the deuteron has two nucleons, a higher energy deposit relative to the proton can be obtained. This enables the evaporation of a larger number of nucleons, resulting in an increase of σ_d/σ_p.

To demonstrate the potential of spallation on the transmutation of LLFP, we estimate the total cross sections on proton and deuteron. By integrating the distributions in Figs. 2 and 4, the respective integral cross sections for the proton and deuteron were determined to be 1110(17) mb and 1300(15) mb for ^{137}Cs,

and 785(10) mb and 998(10) mb for ^{90}Sr. These values are already larger than their thermal neutron-capture cross sections of 270 mb [6] and 10 mb [7], suggesting the spallation reaction is a promising mechanism for the transmutation of these two LLFP nuclei. The PHITS calculations on these integral cross sections for the proton and deuteron are 1157 mb and 1404 mb for ^{137}Cs, and 870 mb and 1094 mb for ^{90}Sr, showing an agreement with the experimental values. Although the present work focuses on a limited region, the tendencies in Fig. 6 indicate that a larger total cross section is expected for the deuteron. Indeed, according to PHITS, the total cross sections on the proton and deuteron are 1190 mb and 1587 mb for ^{137}Cs, and 897 mb and 1255 mb for ^{90}Sr, respectively. In addition, since σ_d is higher on the neutron-deficient side, more neutrons can be produced by the deuteron beam. These neutrons may induce the secondary reactions in the nuclear waste for further transmutation. It appears that the deuteron is also a potential candidate for the LLFP transmutation.

To evaluate the reduction of the radiotoxicities after the spallation reactions, two points are important: the number of LLFP nuclei created in the reaction, and the half lives of these created LLFP nuclei. The long-lived isotopes ^{135}Cs and ^{79}Se are the main components of radioactive decays following the spallation of ^{137}Cs and ^{90}Sr, respectively. Their production cross sections from ^{137}Cs and ^{90}Sr on proton are 64 and 1 mb, respectively. Considering the total reaction cross sections for both ^{137}Cs and ^{90}Sr are around 1 b, the number of LLFP elements can be reduced considerably after the spallation reaction. In addition, ^{135}Cs and ^{79}Se have long half lives of 2.3×10^6 and 6.5×10^4 years [5], respectively. Therefore, the spallation reactions will lead a reduction of the radiotoxicity of the spent fuel.

4. Summary

In summary, spallation cross sections have been measured for the fission products ^{137}Cs and ^{90}Sr on proton and deuteron at 185 MeV/nucleon in inverse kinematics. The σ_d/σ_p ratio increases with the number of protons removed, as well as towards the neutron-deficient side. The experimental data are generally reproduced well by the PHITS code, which includes both the intra-nuclear cascade and evaporation processes. Both proton- and deuteron-induced spallation reactions are promising for the transmutation of ^{137}Cs and ^{90}Sr due to the large total cross sections. Studies on the spallation of other LLFP nuclei are desired for a systematic investigation on their transmutation. Also, the cross sections at low reaction energies are of interest in order to investigate the energy dependence. Further improvements of PHITS as well as other spallation models [35] are desired for their applications to the evaluation of nuclear data as well as the prediction for the neutron contribution in the spallation. The present work is the first attempt in the history of nuclear physics for the treatment on the long-lived fission products. World-wide activities in nuclear physics as well as nuclear engineering may be driven by our initiative. Reaction studies for other long-lived fission products will be triggered by the present study [36].

Acknowledgements

We express our gratitude to the accelerator staff of RIKEN Nishina Center for providing the intense ^{238}U primary beam. We thank K.-H. Schimdt and his co-authors for the help on the SPACS calculation. We thank Dr. D. Steppenbeck for proofreading this article. H.W. acknowledges the financial support from the Foreign Postdoctoral Researcher program of RIKEN. This work is supported by the grant MEXT Nuclear System Research and Development Program.

References

[1] Implication of Partitioning and Transmutation in Radioactive Waste Management, IAEA Technical Reports Series No. 435, 2004.
[2] Potential Benefits and Impacts of Advanced Nuclear Fuel Cycles with Actinide Partitioning and Transmutation, NEA No. 6894, 2009.
[3] W. Wlazło, et al., Phys. Rev. Lett. 84 (2000) 5736.
[4] T. Enqvist, et al., Nucl. Phys. A 703 (2002) 435.
[5] W.S. Yang, et al., Nucl. Sci. Eng. 146 (2004) 291.
[6] H. Wada, et al., J. Nucl. Sci. Technol. 37 (2000) 827.
[7] S. Nakamura, et al., J. Nucl. Sci. Technol. 38 (2001) 1029.
[8] A. Hermanne, J. Nucl. Sci. Technol. 39 (Suppl. 2) (2002) 1202.
[9] T. Kase, et al., J. Nucl. Sci. Technol. 30 (1993) 911.
[10] T. Kubo, Nucl. Instrum. Methods B 204 (2003) 97.
[11] T. Kubo, et al., Prog. Theor. Exp. Phys. 2012 (2012) 03C003.
[12] H. Okuno, N. Fukunishi, O. Kamigaito, Prog. Theor. Exp. Phys. 2012 (2012) 03C002.
[13] T. Ohnishi, et al., J. Phys. Soc. Jpn. 79 (2010) 073201.
[14] N. Fukuda, et al., Nucl. Instrum. Methods B 317 (2013) 323.
[15] Y. Maeda, et al., Nucl. Instrum. Methods A 490 (2002) 518.
[16] A.S. Goldhaber, Phys. Lett. B 53 (1974) 306.
[17] K. Van Bibber, et al., Phys. Rev. Lett. 43 (1979) 840.
[18] L. Giot, et al., Nucl. Phys. A 899 (2013) 116.
[19] T. Nakamura, et al., Phys. Rev. Lett. 103 (2009) 262501.
[20] K. Kobayashi, Master thesis, Rikkyo University, 2012.
[21] J.A. Alcántara-Núñez, et al., EPJ Web Conf. 8 (2010) 07012.
[22] K. Sümmerer, B. Blank, Phys. Rev. C 61 (2000) 034607.
[23] C. Schmitt, K.-H. Schmidt, A. Kelić-Heil, Phys. Rev. C 90 (2014) 064605.
[24] T. Sato, et al., J. Nucl. Sci. Technol. 50 (2013) 913.
[25] A. Boudard, J. Cugnon, S. Leray, C. Volant, Phys. Rev. C 66 (2002) 044615.
[26] S. Furihata, Nucl. Instrum. Methods B 171 (2000) 251.
[27] J. Benlliure, et al., Phys. Rev. C 78 (2008) 054605.
[28] M. Mocko, et al., Phys. Rev. C 76 (2007) 014609.
[29] K. Sümmerer, Nucl. Instrum. Methods B 204 (2003) 278.
[30] M.V. Ricciardi, et al., Nucl. Phys. A 733 (2004) 299.
[31] M. De Jong, A.V. Ignatyuk, K.-H. Schmidt, Nucl. Phys. A 613 (1997) 435.
[32] S. Kox, et al., Nucl. Phys. A 420 (1984) 162.
[33] J.A. Alcántara-Núñez, et al., Phys. Rev. C 92 (2015) 024607.
[34] R.J. Glauber, in: Lectures in Theoretical Physics, vol. 1, Interscience, New York, 1959, p. 315.
[35] J.-C. David, D. Filges, S. Leray, G. Mank, N. Otsuka, Y. Yariv, http://www-nds.iaea.org/spallations/.
[36] http://www.jst.go.jp/impact/en/program08.html.